ARCHIVIO ISTITUZIONALE
DELLA RICERCA

Alma Mater Studiorum Università di Bologna
Archivio istituzionale della ricerca

Nonlinear finite and discrete element simulations of multi-storey masonry walls

This is the final peer-reviewed author's accepted manuscript (postprint) of the following publication:

*Published Version:*
Occhipinti G., Calio I., D'Altri A.M., Grillanda N., de Miranda S., Milani G., et al. (2022). Nonlinear finite and discrete element simulations of multi-storey masonry walls. BULLETIN OF EARTHQUAKE ENGINEERING, 20, 2219-2244 [10.1007/s10518-021-01233-7].

*Availability:*
This version is available at: https://hdl.handle.net/11585/855802 since: 2022-02-10

*Published:*

DOI: http://doi.org/10.1007/s10518-021-01233-7

*Terms of use:*

Some rights reserved. The terms and conditions for the reuse of this version of the manuscript are specified in the publishing policy. For all terms of use and more information see the publisher's website.

This item was downloaded from IRIS Università di Bologna (https://cris.unibo.it/).
When citing, please refer to the published version.

(Article begins on next page)

15 August 2024

# Nonlinear Finite and Discrete element simulations of multi-storey masonry walls

Giuseppe Occhipinti[1*], Ivo Caliò[2], Antonio M. D'Altri[3], Nicola Grillanda[4], Stefano de Miranda[3], Gabriele Milani[4], Enrico Spacone[5]

[1] Institute of Environmental Geology and Geoengineering (IGAG), Italian National Research Council (CNR), Rome, Italy;
[2] Department of Civil Engineering and Architecture(DICAR), University of Catania, via Santa Sofia 64, 95123 Catania, Italy;
[3] Department of Civil, Chemical, Environmental, and Materials Engineering (DICAM), University of Bologna, Viale del Risorgimento 2, Bologna 40136, Italy;
[4] Department of Architecture, Built Environment and Construction Engineering, Technical University of Milan, Piazza Leonardo da Vinci 32, 20133 Milan, Italy
[5] Department of Engineering and Geology, University G. D'Annunzio of Chieti-Pescara, Pescara, Italy

*corresponding author: giuseppe.occhipinti@igag.cnr.it

ABSTRACT

This paper reports the results of different finite and discrete element simulations on a well-known benchmark of an unreinforced plane masonry structure. Namely, the case study concerns a five floor structural wall, located at the interior of a masonry building, situated in "via Martoglio" in the city of Catania (Italy). The numerical simulations aim to investigate the structural response of the wall subjected to seismic actions by means of a non-linear static analyses. The role of reinforced concrete floor beams within URM walls, their influence on the spandrel elements capacity and the approximation that can affect the model if the concrete beam non linearity is not engaged are considered. The benchmark is investigated considering three different structural layouts that have been analysed by means of four numerical approaches. The modelling strategies that have been considered are adaptive NURBS kinematic limit analysis, planar discrete macroelements DME, continuum nonlinear FEM methods and a nonlinear FEM micro-modelling. The results are compared in terms of capacity curves and damage mechanism for each structural layout. As a result, pushover curves and damage patterns appear considerably influenced by the concrete floor beams and their mechanical behaviour. All the considered models denote satisfactory agreement in term of strength and collapse mechanisms, some minor differences are observed in terms of global ductility.

*Keywords*: Masonry buildings, Pushover, Nonlinear Analysis, Micro Model, discrete macro element method, DMEM, FEM, limit analysis.

## 1. Introduction

Multi-storey masonry buildings represent a great percentage of the building stock in several countries. A significant part of these buildings belongs to high seismic prone regions and, as a consequence, it is important to proceed to their seismic assessment for which reliable numerical methods are needed [1]. The benchmark considered in this paper represents typical building in the high seismic region of Catania, an Italian city located in the oriental side of Sicily. Catania represents one of the most vulnerable city all around the world with respect to seismic events. For this reason at the end of the nineties it has been selected for a national research project named Catania Project [2] devoted to the evaluation of the seismic risk in oriental Sicily and particularly in Catania. The *via Martoglio wall*, has been identified as benchmark within the Catania project. It is an interior wall of a five storey masonry building located in the historical centre of Catania. *Via Martoglio wall*, has been investigated by several researchers [3, 4, 5, 6] during the last decades. More recently, the same benchmark has been selected for comparing different computational strategies within the ReLUIS research program funded

by Italian Civil Protection [7, 8]. In this paper, some of the results obtained within the ReLUIS project are collected and discussed. Accordingly, the nonlinear behaviour of the multi-storey wall is analysed by means of mass-proportional pushover analyses performed through different computational models. The comparison involves advanced numerical modelling approaches, namely nonlinear limit analysis [9], planar discrete macroelements DME [3], continuum nonlinear FEM methods [10] and detailed nonlinear FEM micro-modelling [11]. The benchmark has been investigated considering different structural layouts, in particular the influence of the presence of elastic or inelastic floor beams leading to three main structural schemes. The obtained results are compared and discussed in terms of capacity curves and damage scenarios. A good agreement between the different modelling strategies has been observed providing a cross validation between the different considered models. The adopted numerical modelling approaches have been adopted for comparing 3D structures within the same research project [12, 13].

All the results arise important recommendations and warning messages that have to be considered for obtaining a reliable seismic assessment on masonry buildings.

## 2. The benchmark: *Via Martoglio* Building

The benchmark under investigation is inspired to a masonry wall of an URM multi-storey building, placed in the city of Catania (Italy) Figure 1, that was the subject of some previous numerical investigations [3, 4, 5, 6].

Figure 1 View of the inspiring building placed in Catania, Italy.

The wall, identified in Figure 2, is made by regular unit masonry bricks [2] and is characterised by a 300 mm thick except at the last level where the thickness is 160 mm. The 300 mm thick dimension is related to a two wythes interlocked brick layers covered by the external plaster layers while the 160 mm dimension identify the total thickness of a single wythe plastered brick wall.

A regular arrangement of rectangular openings (Figure 3) defines the geometry at all levels with the exception of the ground floor level where a large central door is placed.

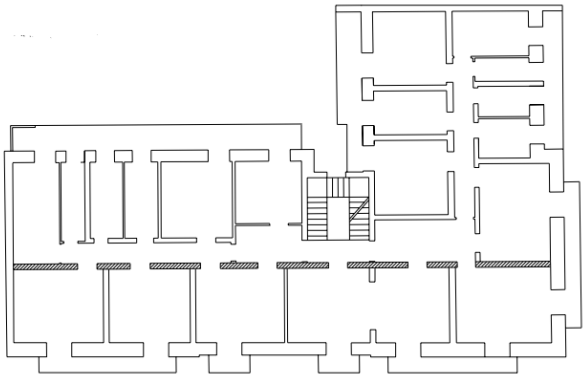

Figure 2 Building plan [2]

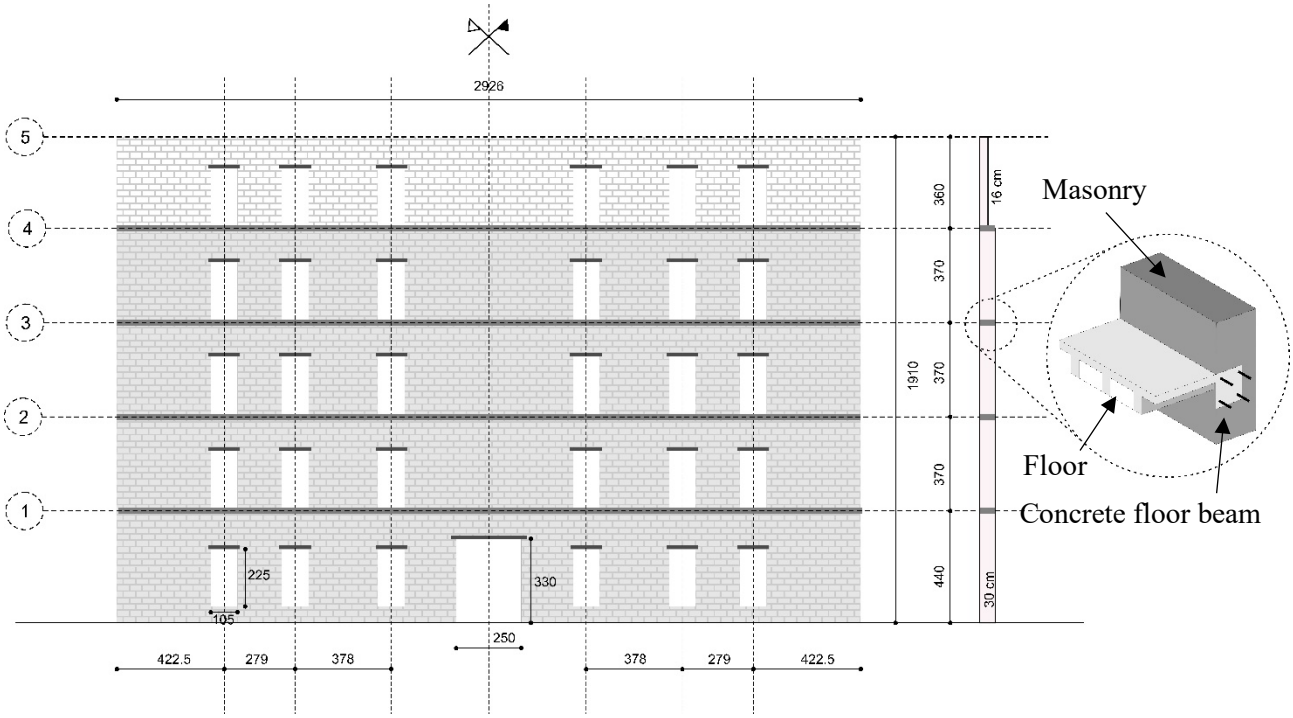


Figure 3 Benchmark multi storey wall and floor sketch.

Some differences can be noticed between the original wall and the benchmark adopted in this work. For instance, in this research the wall is perfectly symmetric respect to the mid axis, [8], in contrast to the original investigated benchmark [3, 4, 5, 6]. All the openings are 105x225mm$^2$ at each level. The main door is 256x330 mm$^2$. Concrete lintels, with 14.5 cm height and 30 cm width, are placed above all the openings. Floor concrete beams of 24 cm height and 30 cm width are placed at each level, except the last one. According to engineering practice of the period of construction the concrete beam has been assumed to be reinforced by 4Ø12 longitudinal bars and Ø6 at 25 cm stirrups, uniformly distributed. Linear elastic concrete lintels, connected to the masonry for 30 cm, are considered for all the openings. The mechanical properties of masonry, concrete beams, steel bars and lintels are summarised in Table 1, Table 2, Table 3 and Table 4 , respectively.

Table 1 Masonry mechanical properties

| Property | Symbol | Unit | Value |
|---|---|---|---|
| Young's Modulus | $E_m$ | MPa | 1600 |
| Shear Modulus | $G_m$ | MPa | 540 |
| Mass Density | $\gamma_m$ | kN/m$^3$ | 17 |
| Compressive Strength | $f_m$ | MPa | 6 |
| Tensile Strength | $f_t$ | MPa | 0.24 |
| Shear Strength | $\tau_{0m}$ | MPa | 0.16 |
| Friction Coefficient | $\mu$ | - | 0.5 |
| Cohesion | c | MPa | 0.15 |
| Brick Tensile Strength | $f_{tb}$ | MPa | 1 |

Table 2 Concrete material properties

| Property | Symbol | Unit | Value |
|---|---|---|---|
| Young's Modulus | $E_c$ | MPa | 28821 |
| Shear Modulus | $G_c$ | MPa | 12009 |
| Poisson's coefficient | $\nu_c$ | - | 0.2 |
| Mass Density | $\gamma_c$ | kN/m$^3$ | 25 |
| Average Compressive Strength | $f_{cm}$ | MPa | 24.6 |
| Tensile Strength | $f_{ct}$ | MPa | 2.169 |
| Limit Strain (model A - NTC18 [14]) | $\varepsilon_{c2}$ | % | 0.2 |
| Ultimate Strain | $\varepsilon_{cu}$ | % | 0.35 |

Table 3 Reinforcement bars material properties

| Property | Symbol | Unit | Value |
|---|---|---|---|
| Young's Modulus | $E_s$ | MPa | 210000 |
| Mass Density | $\gamma_s$ | kN/m$^3$ | 78.5 |
| Yielding limit stress | $f_{yk}$ | MPa | 335 |
| Yielding limit strain | $\varepsilon_{sy}$ | % | 0.23 |

Table 4 Lintel beams elastic properties

| Property | Symbol | Unit | Value |
|---|---|---|---|
| Young's Modulus | $E_l$ | MPa | 28821 |
| Poisson's coefficient | $\nu_l$ | * | 0.2 |
| Mass Density | $\gamma_l$ | kN/m$^3$ | 17 |

All the numerical models consider besides the self-weight load distributions consider distributed linear loadings associated to the to the floor slabs directly applied at each level as summarised in Table 5.

Table 5 Loads at each level

| Level | 1 | 2 | 3 | 4 | 5 |
|---|---|---|---|---|---|
| Qtot [kN] | 286 | 353 | 353 | 345 | 53 |

Three different configurations have been considered for the comparison between the adopted numerical approaches as specified in the following:

- Configuration1 - URM wall, characterised by uniform mechanical properties reported in Table 1 without floor beams.

- Configuration2 - Masonry wall equal to Configuration1 with elastic floor floor beams at each level except the last one.
- Configuration3 - Masonry wall with equal to Configuration2 that considers nonlinearity in concrete beams.

The three considered configurations have been analysed by means of the four numerical approaches that are characterised by different level of sophistication and modelling strategies. All the configurations have been analysed by mass-proportional pushover analyses.

In the following a brief description of the adopted modelling strategies is reported, the interested reader can find more details in the referenced papers.

## 3. The modelling strategies

Four modelling strategies have been adopted for the comparisons. Two are based on nonlinear FEM analyses at the macro and micro-scale, one is based on a discrete macro-element model and the fourth is based on a kinematics limit analysis procedure based on collapse mechanisms, associated to very rigid elements, iteratively adjusted to minimize the load multiplier.

### 3.1 Discrete macro-element method DMEM

The DMEM here applied [3, 15] is based on the use of a plane discrete macro element able to simulate the main in-plane collapse mechanisms of masonry walls subjected to vertical and horizontal loadings, Figure 4.

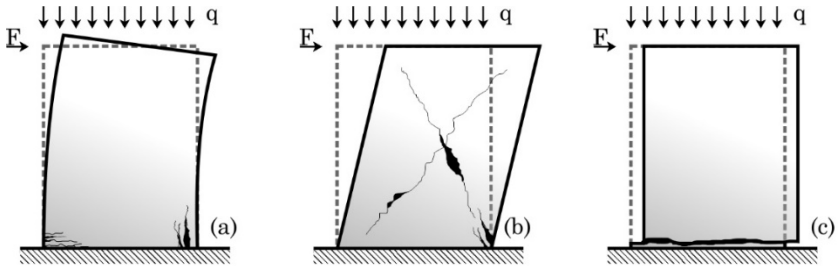


Figure 4 Main in-plane failure mechanisms of a masonry portion (a) flexural failure; (b) shear-diagonal failure; and (c) shear sliding failure.

The plane element can be described by referring to a simple mechanical representation in which the element is regarded as a plane articulated quadrilateral endowed with alongside nonlinear zero-thickness interfaces. The mechanical behaviour of the element is governed by alongside nonlinear interfaces and the in-plane deformability of the quadrilateral whose behaviour is related to a single degree of freedom calibrated according to uniaxial constitutive law. In order to adopt a straightforward fibre discretization, the zero-thickness interfaces have been conveniently represented in Figure 5.a as a regular distribution of nonlinear links orthogonal to the interfaces.

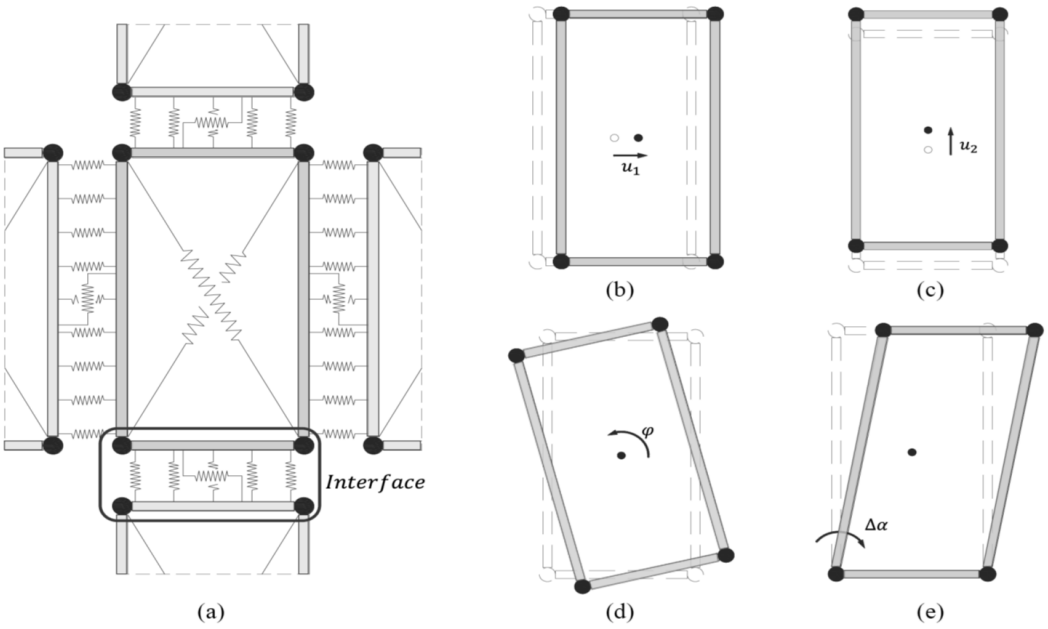


Figure 5 Two-dimensional macro-element: (a) mechanical scheme, (b, c, d, and e) the needed Lagrangian parameters for the kinematics description according to a discrete element approach.

The shear sliding behaviour along the interfaces, associated to relative motion in the direction of the interface, can be efficiently described through a single longitudinal spring. The kinematics of the mechanical scheme, after a proper calibration procedure of the nonlinear links, is capable of simulating the main in-plane collapse failure modes of a masonry panel: flexural failure, diagonal shear failure and sliding shear failure Figure 6.

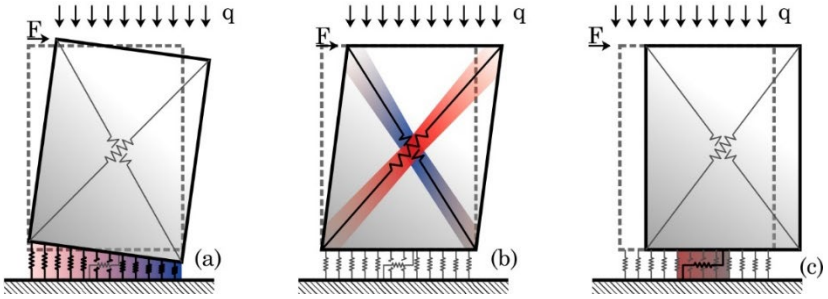


Figure 6 Simulation of the main in-plane failure mechanisms of a masonry portion by means of the considered plane discrete macro-element: (a) flexural failure; (b) shear-diagonal failure; and (c) shear sliding failure.

In spite of its simplicity, the assemblage of these elements allows the simulation of the global nonlinear response of masonry buildings, however in the plane model the out-of-plane response of the masonry walls is not taken into account.

Each discrete-element exhibits three degrees-of-freedom associated to the in-plane rigid body motion, plus an additional degree-of-freedom, needed for the description of the in-plane shear deformability (see Figure 5.b, Figure 5.c, Figure 5.d and Figure 5.e). The deformations of the interfaces are associated to the relative motion between corresponding panels; therefore, no further Lagrangian parameter has to be introduced in order to describe the model kinematics. The adopted model has the advantage of interacting with the adjacent elements along the whole perimeter, thus allowing the possibility of using different mesh discretization. The calibration of the nonlinear links orthogonal to the interface is associated with the basic mechanical parameters governing the axial/bending behaviour of masonry continuum, the Young's modulus $E$, the compressive $f_c$ and tensile $f_t$ strengths. In addition, a limited ductility, both in tension and compression, can be introduced for these links, after which the force is redistributed to the other contiguous links with remaining resistance sources.

Consistently with a crack and crush model, if the achieving of the ultimate ductility occurs in tension, the link holds the possibility to bear a compressive force; on the other hand, the achieving of the ultimate compressive ductility implies the complete loss of the bearing capacity of the link. In addition, the occurrence of combined failure mechanisms can be caught Constitutive laws more sophisticated and related to cyclic degrading softening behaviour, can also be considered for nonlinear dynamic analyses [16]

In the DMEM model, the orthotropic flexural behaviour of masonry (Figure 7A) is simulated by means of the orthogonal link along the entire perimeter of the quadrilateral. Each link encompasses the axial behaviour of the corresponding fibre along the given material direction (Figure 7B). With a regular macro-element, each link is calibrated, assuming that the uniform masonry strip is a homogeneous inelastic material. The initial stiffness K, compressive and tensile yield strengths, fc and ft, and the ultimate displacements, $u_c$ and $u_t$, are evaluated as reported in Table 1. The Young's moduli, $E_h$ and $E_v$, of a typical homogenized orthotropic masonry medium, $\sigma_{ch}$, $\sigma_{th}$, and $\sigma_{cv}$, $\sigma_{tv}$ are the corresponding compressive and tensile maximum stresses, $G_{ch}$, $G_{th}$, and $G_{cv}$, $G_{tv}$ are the fracture energies in compression and tension, as shown in Figure 10a, related to a post-peak linear softening branch.

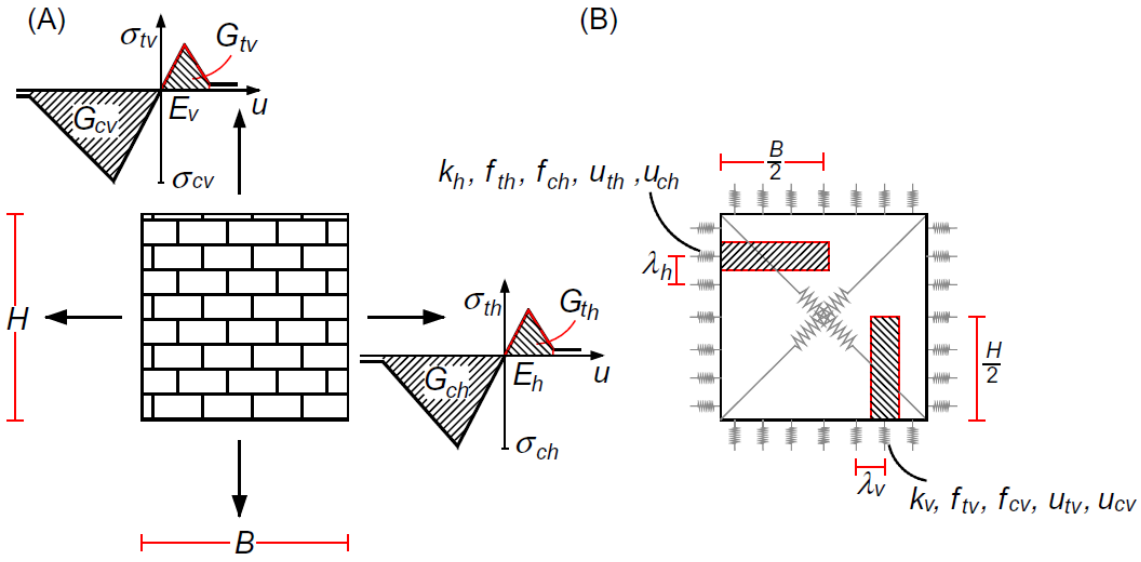


Figure 7 Mechanical characterization of an orthotropic masonry panel: (A) constitutive laws; (B) calibration of the orthogonal links (Pantò et al., 2017a).

Table 6 Mechanical calibration of the orthogonal links of a regular DMEM model

| Direction | $K$ | $f_c$ | $f_t$ | $u_c$ | $u_t$ |
|---|---|---|---|---|---|
| Horizontal | $K_h = 2\frac{E_h\lambda_h\lambda_s}{B}$ | $f_{ch} = \sigma_{ch}\lambda_h\lambda_s$ | $f_{th} = \sigma_{th}\lambda_h\lambda_s$ | $u_{ch} = 2\frac{G_{ch}}{\sigma_{ch}}$ | $u_{th} = 2\frac{G_{th}}{\sigma_{th}}$ |
| Vertical | $K_v = 2\frac{E_v\lambda_v\lambda_s}{H}$ | $f_{cv} = \sigma_{cv}\lambda_v\lambda_s$ | $f_{tv} = \sigma_{tv}\lambda_v\lambda_s$ | $u_{cv} = 2\frac{G_{cv}}{\sigma_{cv}}$ | $u_{tv} = 2\frac{G_{tv}}{\sigma_{tv}}$ |

Although the model allows obtaining an orthotropic calibration of the macro-element, in the application reported in the following in order to be consistent with the other approaches at the macro-scale, an isotropic behaviour has been assumed for all the masonry material.

The sliding behaviour is usually rigid-plastic with yielding criteria associated to a Mohr-Coulomb domain. For each interface, the corresponding axial force is that acting on the corresponding transversal links. Due to the low computational burden, this model allows to model efficiently not only unreinforced masonry structures, but also mixed reinforced concrete- (or steel-) masonry structures [17]. In this paper, the plane model is employed, considering the interaction between the masonry panels and the concrete floor beams. The beams have been modelled considering a concentrated plasticity frame element [18]. The adopted mechanical parameters are coherent with Table 1, Table 2, Table 3 and Table 4 and rearranged in the following tables.

196 Table 7 Resistance parameters adopted in the model - masonry

| Property | Symbol | Unit | Value |
|---|---|---|---|
| Masonry Elastic Module | Em | MPa | 1600 |
| Masonry Compressive Strength | fm | MPa | 6 |
| Masonry Tensile Strength | ft | MPa | 0.24 |
| Tensile Ductility | | - | 1.05 |
| Compressive Ductility | | - | ∞ |
| Masonry Shear Module | G | MPa | 540 |
| Friction coefficient | $\mu$ | - | 0.5 |
| Shear Strength | $\tau_0$ | MPa | 0.16 |
| Mass Density | $\gamma_m$ | kN/m3 | 17 |

197

198 Table 8 Resistance parameters adopted in the model - concrete

| Property | Symbol | Unit | Value |
|---|---|---|---|
| Concrete Elastic Module | Ec | MPa | 28821 |
| Poisson's Coefficient | v | - | 0.2 |
| Compression Strength | fc | MPa | 24.6 |
| Tensile Strength | ft | MPa | 2.169 |
| Limit Strain (model A - NTC18 [14]) | $\varepsilon c2$ | % | 0.2 |
| Ultimate Strain | $\varepsilon u$ | % | 0.35 |
| Mass Density | $\gamma_c$ | kN/m$^3$ | 25 |

199

200 Table 9 Resistance parameters adopted in the model - reinforcements

| Property | Symbol | Unit | Value |
|---|---|---|---|
| Bars Elastic Module | Es | MPa | 210000 |
| Poisson's Coefficient | v | - | 0.2 |
| Yielding limit stress | $f_{yk}$ | MPa | 335 |
| Ultimate Strain | $\varepsilon_u$ | % | 0.23 |
| Mass Density | $\gamma_s$ | kN/m$^3$ | 78.5 |

201

202 Table 10 Resistance parameters adopted in the model - lintel

| Property | Symbol | Unit | Value |
|---|---|---|---|
| Bars Elastic Module | $E_l$ | MPa | 30000 |
| Poisson's Coefficient | v | - | 0.2 |
| Mass Density | $\gamma_l$ | kN/m$^3$ | 25 |

203
204
205

## 206 3.2 Limit analysis based model

207 The kinematics limit analysis based model [9] is applied to a model composed of few rigid elements in
208 which the initial discretization is iteratively adjusted aiming to minimize the kinematic load multiplier. The
209 wall is represented by 2D rectangular NURBS (Non-Uniform Rational Bezier Spline) plate elements. Macro-
210 blocks are derived by assigning a thickness value to each plate element. Each macro-block is considered
211 infinitely rigid and resistant. This assumption allows representing the kinematics in terms of the three degrees
212 of freedom of the centroid. The internal dissipation is allowed only on the common boundaries between
213 adjacent elements where the interfaces are defined. The amount of internal dissipation is computed by
214 assuming a rigid-plastic behaviour and a 3D yielding domain that represents a Mohr-Coulomb criterion with
215 tension cut-off and linear cap in compression (see Figure 8).

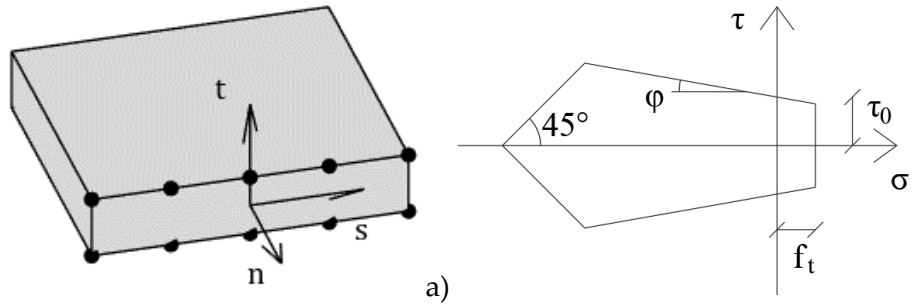


Figure 8. (a) 3D view of a single macro-block, interface discretization, and local reference system, (b) section of the 3D Mohr-Coulomb yielding domain.

By applying a standard kinematic limit analysis procedure, which can be summarized into a linear programming (LP) problem, load multiplier and mechanism are calculated. The mechanism is defined in terms of a discontinuous velocity field, where velocity jumps occur at the interfaces according to an associative flow rule (Eq. 1).

$$\min\left\{\lambda = \mathbf{c}\dot{\boldsymbol{\lambda}} - \mathbf{f}_d\dot{\mathbf{u}}\right\} \text{ such that } \begin{cases} \mathbf{A}\dot{\mathbf{u}} - \mathbf{B}\dot{\boldsymbol{\lambda}} = 0 \\ \mathbf{f}_L\dot{\mathbf{u}} = 1 \\ \dot{\boldsymbol{\lambda}} \geq 0 \end{cases} \quad \text{Eq. 1}$$

where $\lambda$ is the load multiplier, $\dot{\mathbf{u}}$ represents the discontinuous velocity field, $\dot{\boldsymbol{\lambda}}$ are the non-negative plastic multipliers at interfaces, $\mathbf{c}$ is the vector representing the amount of internal dissipation, $\mathbf{f}_d$ and $\mathbf{f}_L$ are respectively the vectors of dead- (permanent) and live-loads, and finally $\mathbf{A}$ and $\mathbf{B}$ are the matrices for the imposition of the compatibility constraints (i.e. the associative flow rule).

The discretisation of the wall by few blocks makes the result affected by the initial mesh and, consequently, leads to an inaccurate collapse mechanisms as well as the associated kinematic multiplier, being an upper bound of the real collapse one. Due to these issues, a mesh adaptation procedure is always applied. The initial mesh is iteratively adjusted by modifying the elements shape until interfaces coincide with the real fracture lines. With this aim, a meta-heuristic approach based on a Genetic Algorithm [19] (GA) is adopted. Mesh modifications are even facilitated in models realized through the NURBS geometry, in which subdividing of moving operations can be conducted in easy way [20, 21, 22].

The multi-storey wall has been studied under the application of a configuration of horizontal load proportional to masses (i.e. self-weights and the non-structural masses applied). The resistance parameters adopted are reported in Table 11.

Table 11 Resistance parameters adopted in the model

| Parameter | Value |
|---|---|
| Compression strength | fc = 6 MPa |
| Tensile strength | ft = 0 MPa |
| Cohesion | τ0 = 0.16 MPa |
| Friction angle | φ = 27° for horizontal interfaces<br>= 45° for diagonal interfaces<br>= 67° for vertical interfaces |

Differently from other models, that considered the parameters in Table 1, a null value of tensile strength has been here adopted. Indeed, considering the rigid-plastic behaviour assumed in the limit analysis tool, and consecutively the impossibility to take into account the softening behaviour in tension through a LP formulation, the behaviour of the in-plane loaded wall resulted better represented by using a null value of tensile strength. Moreover, with the aim of taking into account the dilatancy effects due also to the disposition of bricks, different values of friction angle have been assigned for diagonal and vertical interfaces, i.e. interfaces that do not coincide with mortar bed joints (see Table 11).

### 3.3 The homogeneous isotropic plastic-damaging 3D continuum model

The nonlinear FEM model at the macro-scale is based on a homogeneous isotropic plastic-damaging 3D continuum. Such plastic-damage model, firstly developed by Lee and Fenves [10], hypothesizes independent tensile and compressive behaviours ruled by tensile damage ($0 \leq d_t < 1$) and compressive damage ($0 \leq d_c < 1$) variables. Thus, the uniaxial stress-strain curves can be described by:

$$\sigma_t = (1-d_t)E(\varepsilon_t - \varepsilon_t^p) \quad \text{Eq.2.a}$$

$$\sigma_c = (1-d_c)E(\varepsilon_c - \varepsilon_c^p) \quad \text{Eq. 2.b}$$

where $\sigma_t$ is the uniaxial tensile stress, $\sigma_c$ is the uniaxial compressive stress, $E$ is masonry Young's modulus, $\varepsilon_t$ and $\varepsilon_c$ are the uniaxial tensile and compressive strains, respectively, and $\varepsilon_t^p$ and $\varepsilon_c^p$ are the uniaxial tensile and compressive plastic strains, respectively (Eq. 2.a and Eq. 2.b). Consequently, the uniaxial stress-strain curves shown in Figure 9 represent the main input for the model mechanical characterization. The masonry mechanical properties used in this study are collected in Table 12.

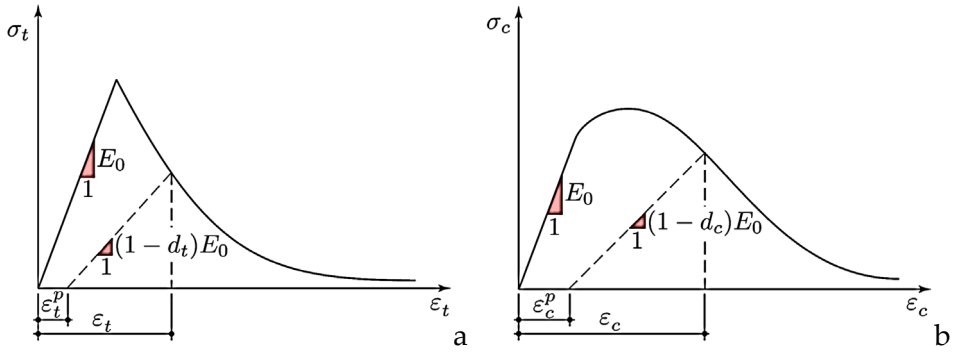


Figure 9 Nonlinear behaviour: (a) tensile and b) compressive uniaxial stress-strain curves.

| | | |
|---|---|---|
| Density [kg/m³] | 1700 | |
| Young's modulus $E$ [MPa] | 1300MPa | |
| Poisson's coefficient $\nu$ | 0.2 | |
| Compressive behaviour | | |
| Stress [MPa] | Inelastic strain | $d_c$ |
| 6.0 | 0 | 0 |
| 6.0 | 0.003 | 0 |
| 0.6 | 0.01 | 0.9 |
| Tensile behaviour | | |
| Stress [MPa] | Inelastic strain | $d_t$ |
| 0.24 | 0 | 0 |
| 0.02 | 0.001 | 0.9 |

Table 12. Masonry mechanical properties.

In order to manage dilatancy in the material behaviour and to govern the plastic strain rate, a non-associative flow rule is supposed through a Drucker-Prager type plastic potential. Such potential is described by the angle of dilatancy $\psi$, supposed equal to 10° according to [23], and a smoothing constant $\epsilon$ supposed equal to 0.1 according to the literature [24, 25]. A multiple-hardening Drucker-Prager type surface is supposed as yield surface, described by $f_{b0}/f_{c0}$, i.e. the ratio between the biaxial $f_{b0}$ and uniaxial $f_{c0}$ compressive strengths herein supposed $f_{b0}/f_{c0} = 1.16$ [26], and a shape parameter $\rho$ which represents the ratio of the second stress invariant on the tensile meridian to that on the compressive meridian at primary yield, herein supposed $\rho = 2/3$ [26].

Within this study, the 3D continuum that represents masonry is discretized by means of 4-nodes tetrahedral linear FEs, with representative size 0.4 m. In case of presence of reinforced concrete floor beams, the same type of FEs are used to account for these beams (so obtaining a conforming mesh), consequently the linear elastic behaviour is supposed for floor beams. In order to run pushover analyses and to account for possible global softening behaviour, a quasi-static direct-integration implicit dynamic algorithm has been

utilized [25]. Accordingly, this algorithm allows the simulation of quasi-static behaviours, in which inertia is only introduced to regularize unstable responses.

It should be underlined that this constitutive model formerly developed for concrete and isotropic quasi-brittle materials has been widely utilized for masonry structures [24, 27, 28], even though they may present significant anisotropic responses. Although few anisotropic models have been proposed expressly for masonry [29, 30], their use has found some limits due to the many parameters needed to characterize the material. Furthermore, this isotropic model appears capable to efficiently catch both flexural and shear failures of a masonry pier, i.e. the main features that govern the response of masonry structures under horizontal loads [31]. Therefore, the model is expected to be rather accurate for the piers despite the isotropic nature, while higher approximations are expected on the spandrel response (where, however, limited information is still available on failure modes).

### 3.4 The micromodelling approach

The more sophisticated model adopted in this research is a FEM micromodelling approach. From a macroscopic point of view, masonry can be defined as a composite material consisting of microstructural components (bricks and mortar joints) with strongly nonlinear behaviour, whose arrangement within the microstructure leads to very complex nonlinear behaviours characterized by different collapse modes. In the micromodelling approach, the masonry microstructure is explicitly modelled and each microscopic behaviour is described by its own nonlinear constitutive model. The chosen micromodel references the $d^+$ $d^-$ tension/compression damage model based on the continuous model put forward by Cervera et al. 1995 [32], Faria et al. 1998 [33], Wu et al. 2006 [34], and further refined by Petracca et al. [35, 36, 37] to correctly reproduce the nonlinear shear response of masonry walls and to control the effect of dilatancy.

The advantage of micromodelling is obtaining a different response from the masonry wall in tension and compression, and at the same time, being able to describe unilateral effect crack closure correctly.

The bi-dissipative damage model of Cervera et al. 1995 [32], Faria et al. 1998 [33], Wu et al. 2006 [34] defines the effective stress tensor, $\sigma_{eff}$:

$$\sigma_{eff} = (1+d^+)\cdot\bar{\sigma}^+ + (1-d^-)\cdot\bar{\sigma}^- \quad \text{Eq. 3}$$

Where $\sigma_{eff}$ is the effective stress tensor, $\bar{\sigma}^+$ and $\bar{\sigma}^-$ are the positive and negative parts of the effective stress tensor $\sigma_{eff}$ (elastic part), $d^+$ and $d^-$ are, respectively, the tension and compression damage indices and they influence the positive $\bar{\sigma}^+$ and negative $\bar{\sigma}^-$ parts of the effective stress tensor $\sigma_{eff}$ (inelastic part). The damage indices are scalar variables from 0 (intact material) to 1 (completely damaged material).

The damage indices are calculated first by defining damage areas (or damage criteria). Such areas are functions that, given a stress, return a scalar magnitude called equivalent tensile stress. If the equivalent tensile stress ($\tau^+$ - $\tau^-$) assumes a value of zero, the stress is within the strength domain and the material is intact; if it assumes a value greater than zero the material is damaged.

For modelling 2D plane-stress elements with four nodes, the compression surface used is an improvement of that described in Lubliner et al. 1989 [38], where the stresses equivalent to compression and tension are calculated as:

$$\tau^- = H(-\bar{\sigma}_{\min})\left[\frac{1}{1-\alpha}\left(\alpha\bar{I}_1 + \sqrt{3\bar{J}_2} + k_1\beta\langle\bar{\sigma}_{\max}\rangle\right)\right] \quad \text{Eq. 4}$$

$$\tau^+ = H(\bar{\sigma}_{\max})\left[\frac{1}{1-\alpha}\left(\alpha\bar{I}_1 + \sqrt{3\bar{J}_2} + \beta\langle\bar{\sigma}_{\max}\rangle\right)\frac{\sigma_t}{\sigma_p}\right] \quad \text{Eq. 5}$$

$$\alpha = \frac{k_b - 1}{2k_b - 1} \quad \text{Eq. 6}$$

$$\beta = \frac{\sigma_p}{\sigma_t}(1-\alpha) - (1+\alpha) \quad \text{Eq. 7}$$

Where $\overline{\sigma}_{max}$ is the principal effective stress tensor, $\sigma_t$ is the tensile strength of mortar units or joints, $\sigma_p$ is peak compressive strength of mortar units or joints, $I_1$ is the first invariant of the effective stress tensor, $J_2$ is the second invariant of the effective deviatoric stress tensor and $k_b$ is the ratio of the bi-axial strength to the uniaxial strength in compression. Figure 10 graphically represents the described roles.

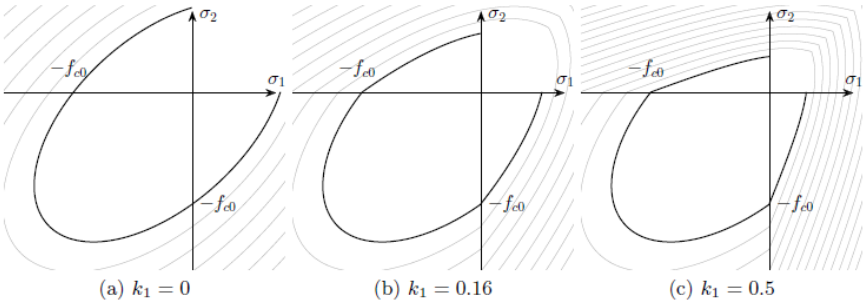


Figure 10 Compressive failure surface of the continuous micromodel [35, 36, 37]

Being the damage an irreversible process, the model introduces the damage threshold $r^+$ and $r^-$, two scalar variables that denote the values attained by the equivalent stresses $\tau^+$ and compressions $\tau^-$ throughout the whole loading history for each time step.

$$r^+(t) = \max(\max_{s\in[0,t]} \tau^+(s); f_t) \qquad \text{Eq. 8.a}$$

$$r^-(t) = \max(\max_{s\in[0,t]} \tau^-(s); f_{c0}) \qquad \text{Eq. 8.b}$$

Once the damage thresholds have been assessed, damage indices $d^+$ e $d^-$can be evaluated.

The indices of damage and the stress and compressive damage evolution are defined through uniaxial tensile-deformation laws, where the degrading section is governed by the values assumed by the compressive $G_c$ and tensile $G_t$ fracture energies.

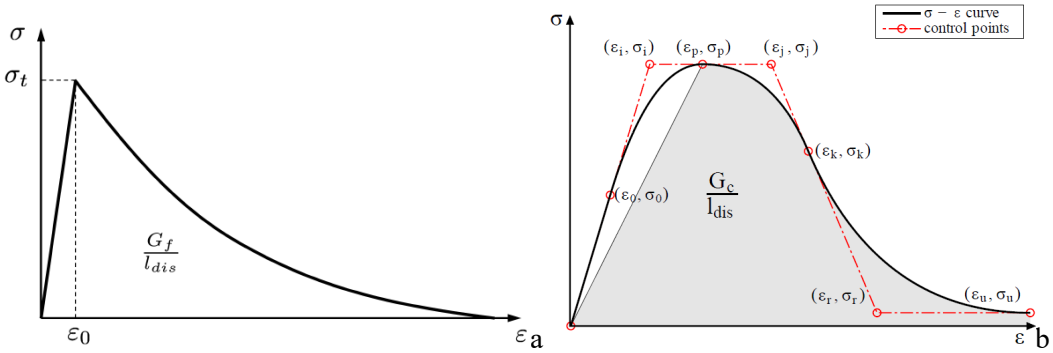


Figure 11 a) Tensile and b) Compressive uniaxial laws [35, 36, 37]

The parameters were obtained through a calibration process of the mechanical properties and the fracture energies of the masonry microstructure.

Table 13 reports the mechanical properties assumed for the quasi-static nonlinear analyses. In the choice of mechanical parameters, it has been considered that the uniaxial compressive strength of mortar joints and brick units are substantially different, with the mortar strength being lower than the brick strength. However, the overall wall equivalent compressive strength is larger than the mortar strength. This is due to the fact that, even if the wall is in an "equivalent" state of plane-stress, its micro-structural constituents are not in the same state due to their different elastic moduli, mainly. It is worth noting that in the reality, the mortar is confined by the surrounding bricks and, consequently, it develops triaxial compression states that increase the resulting strength. This phenomenon is not achieved in the present model, due to the 2D plane-stress assumption at both mortar and brick. To overcome this issue, the compressive strength used for both bricks and mortar joints has been evaluated by matching the equivalence with the actual wall. In Table 13 the assumed mechanical parameters of brick and mortars are summarised.

Table 13 Mechanical parameters taken as reference for numerical analysis a) Mechanical properties of the bricks b) Mechanical properties of the mortar

| Property | Symbol | BRICKS | MORTAR |
|---|---|---|---|
| Elastic Module | Eb [N/mm²] | 3000 | 360 |
| Poisson's Ratio | ν [-] | 0.20 | 0.20 |
| Tensile strength | $\sigma_t$ [N/mm²] | 1.00 | 0.15 |
| Tensile Fracture Energy | $G_t$ [N/mm] | 0.08 | 0.02 |
| Compression strength | $\sigma_0$ [N/mm²] | 4.00 | 4.00 |
| Compressive peak strength | $\sigma_p$ [N/mm²] | 6.00 | 6.00 |
| Residual strength | $\sigma_r$ [N/mm²] | 0.10 | 0.1 |
| Compression Fracture Energy | $G_c$ [N/mm] | 6.00 | 4 |
| Peak deformation | $\varepsilon_p$ [-] | 0.008 | 0.05 |
| Lubliner yield-surface coefficient | $k_b$[-] | 1.15 | 1.15 |
| Dilatancy coefficient | $k_1$[-] | 0.00 | 0.16 |

## 4. On the choice of the adopted mechanical parameters for a consistent comparison

According to the above mentioned computational strategies and aiming to compare the models on simple elements, a square panel (2.5x2.5x0.5 m) have been horizontally loaded under five vertical load levels and two constrain layouts (following a procedure akin to the one proposed in [31]). The considered vertical loads correspond to the 12%, 18%, 30%, 50% and 75% of the compressive limit force. All the results are compared to the flexural and shear domains of the Italian Design Code [14]. The presence, and absence, of rotational restrain is taken into account at the top edge. The two loading tests aim to simulate flexural and shear behaviour that affect an entire multi-storey wall. Figure 12 shows a good agreement between the numerical results as well as the theoretical domains.

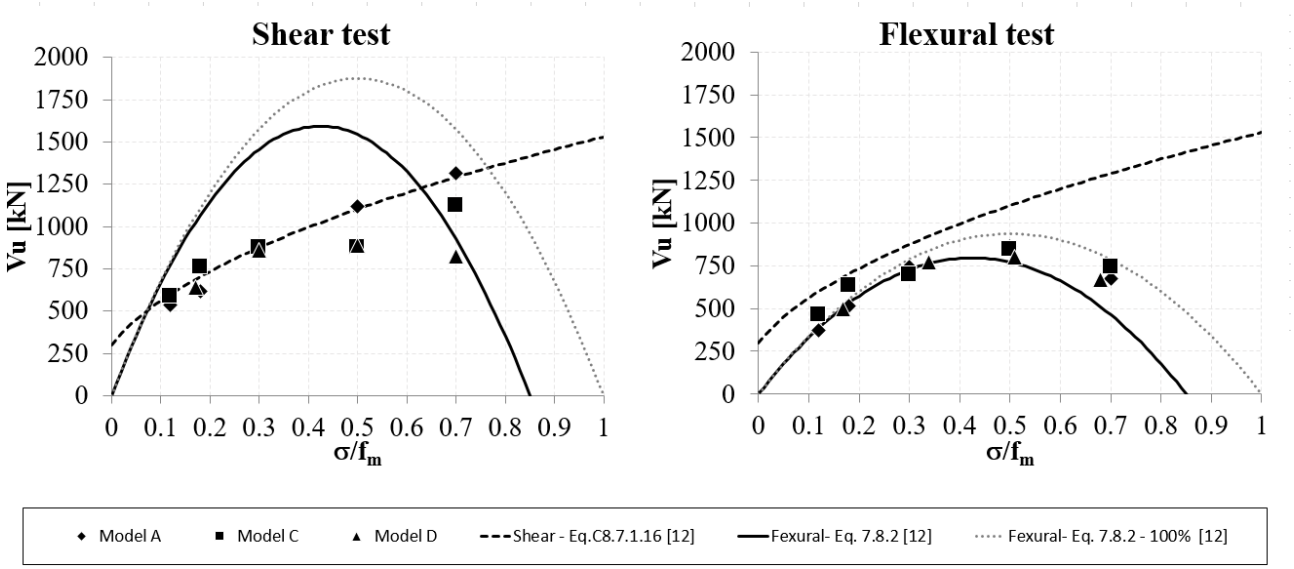


Figure 12 Results of a) shear and b) flexural loading test

However, the comparison does not return any information about tangent stiffness or post peak branch but it allows comparing the peak values. A satisfactory agreement can be observed in the range of 12%-30% that denotes most of real cases.

## 5. Numerical Results

The results of the analyses relative to the three different structural layouts are discussed in the following. Configuration1, in which floor beams are not considered, is characterised by the mechanical properties summarised in Table 1; Configuration2 considers elastic floor beams at each level except to the roof level;

Configuration3 considers nonlinear concrete floor beams and elastic lintel beams. Figure 13 sketches the benchmark and indicates the control points P1 and P2 at top corners of the wall.

The analyses consider mass-proportional load distribution as sketched in Figure 13.

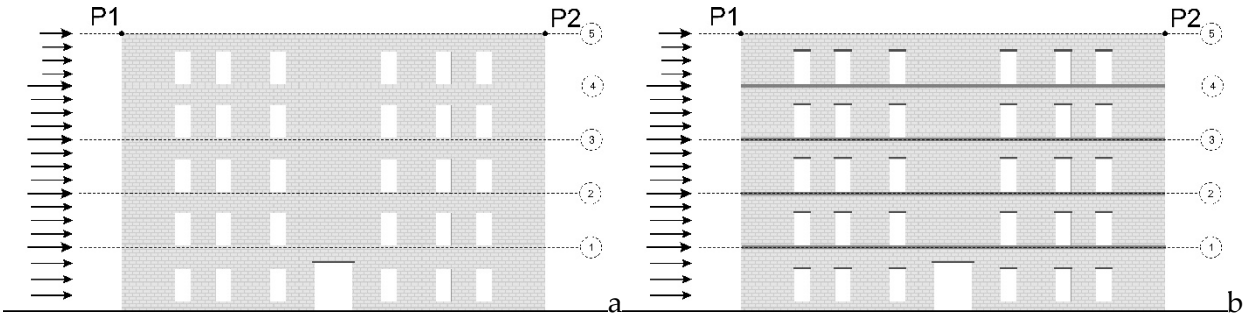


Figure 13 Benchmark scheme and control points a) Configuration1 and b) Configuration2 and Configuration3

Table 14 summarises the used hardware equipment and allows comparing the computational burdens of all methods that have been engaged in this research. As the table shows, the adopted computational models need computational burden that increases with the level of sophistication. Starting from the limit analysis up to the micro-modelling the computational costs increase. In the detailed strategy, partition modelling and multiprocessor features are adopted.

Table 14 Computational burden comparison

| Model | CPU | RAM | Configuration | DOF | Time |
|---|---|---|---|---|---|
| Limit Analysis Based Model | Intel®Core™ i7 5500U 4.20 GHz | 8 Gb | 1-2-3 | 435 | 15 min. |
| Discrete macro-element method DMEM | Intel®Core™ i7 7500U 2.70-2.90 GHz | 16 Gb | 1 | 525 | 4 min. |
| | | | 2 | 1007 | 5 min. |
| | | | 3 | 1007 | 15 min. |
| Homogeneous Isotropic Plastic-Damaging 3D Continuum Model | Intel®Core™ i7-6500U 2.50GHz | 16 Gb | 1 | 41406 | 2 h 20 min |
| | | | 2 | 41406 | 1h 17 min |
| Micromodelling Approach | 24 cores | | 1 | 359536 | 45 min |
| | | | 2-3 | 359536 | 80 min |

The limit analysis model uses rigid blocks with dissipation at interfaces only. Each rigid block has three degrees of freedom: the in-plane translations and the rotation of the centroid. Hence, the total number of degrees of freedom for the optimized mechanism correspond to 435. However, the total amount of unknowns in the linear programming problem (Eq. 1) includes also the non-negative plastic multiplier rates, whose number is equal to the number points involved in the discretization of interfaces multiplied by the number of planes used to linearize the failure domain (17 in this case). Therefore, the total amount of unknowns in the linear programming problem (degrees of freedom and plastic multiplier rates) is equal to 14307. By using a laptop equipped with an Intel®Core™ i7 5500U processor (4.20 GHz) and 8 GB RAM, 5.31 seconds were required to solve the single linear programming problem. In the mesh adaptation procedure, fracture lines were constrained to be horizontal, vertical, or diagonal in order to represent the typical failure mechanisms of in-plane loaded walls: therefore, the iterative procedure required very few iterations, corresponding to the computational time of 15 minutes, globally.

The discrete macro-element method involves 525 degree of freedom in Configuration1, 1007 in Configuration2 and Configuration3. The analyses were carried out on a laptop equipped with Intel®Core™ i7 7500U CPU at 2.70GHz - 2.90 GHz and 16.0 GB RAM. The computing time efforts were 4 minutes for Configuration1, 5 minutes for Configuration2 and 15 minutes for Configuration3. In the latter case, the model takes 5 minutes to reach the drift level at which a reduction of 20% of the peak force is achieved and 10 minutes until the end of the analysis.

The nonlinear FEM model is made of 42272 plane elements and 13803 nodes, with 41406 degree of freedom, totally. Computing times on a laptop with a processor Intel®Core™ i7-6500U CPU at 2.50GHz and 16GB RAM is 2 hours and 20 minutes for Configuration1 and 1 hour and 17 minutes for Configuration2.

The micromodel is made of 359536 degrees of freedom and 176838 4-noded plane stress elements. The solution strategy adopts a mixed implicit-explicit (IMPLEX) algorithm that requires typically 2 or 3 iterations to reach convergence. The analyses run with 24 processors using a parallel computation strategy. The analysis time required is about 45 minutes and 80 minutes for the configuration with and without the RC concrete beam, respectively.

## 5.1 Configuration1 – URM

The present section reports the results that has been obtained for Configuration1. The specimen does not implement floor beams or, even implicitly, the restrain effect offered by the floors. This assumption is coherent with the hypothesis that the floors does not provide a sufficient in-plane constraint on the masonry wall. Consequently, the only connection between the piers is guaranteed by the spandrels.

Figure 14 reports the capacity curves obtained by the three software, based on step-by-step procedures, and the ultimate load provided by the limit analysis based model.

It can be observed a satisfactory agreement between the considered models in terms of ultimate capacity. A small difference can also be observed in terms of residual strength. Two models are characterised by a stiffness reduction range at a similar force level (680 kN, 707 kN respectively). These values correspond to the initiation of damage in the spandrels at the different floors in the software that consider a softening tensile response. One simulation reaches a superior force level but it is characterised by a sensible softening post peak behaviour. The values of the peaks, in increasing order, are 685.1 kN, 786 kN, 834.4 kN, and 838.6 kN. Globally the post-peak branches are characterised by sensible ductility levels that can be evaluated according to the rocking mechanism of the “cantilever mega-pier”.

Of a certain interest is the collapse mechanism reported in Figure 15 although it has to be analysed paying attention to the model assumptions. After a certain level of horizontal displacement, due to the horizontal seismic forces, the tensile strength is progressively reached in the spandrels corresponding to the right side of the wall, this leads to a separation of the façade along vertical lines corresponding to the zone in which the spandrels reached their limits of tensile strength. In this condition the displacements of the two control points are extremely different and in the extreme right position a partially collapse of the masonry occurs.

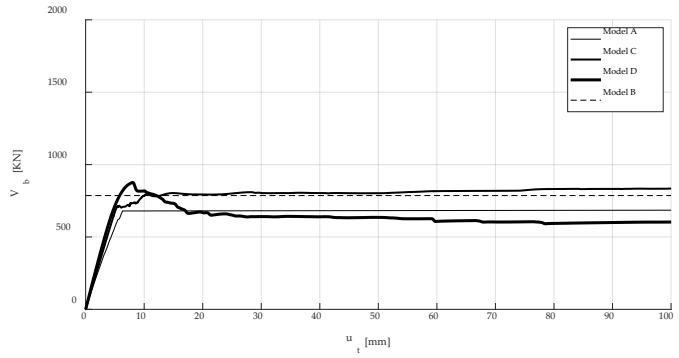


Figure 14 Comparison of the capacity curves obtained with three adopted software for Configuration1

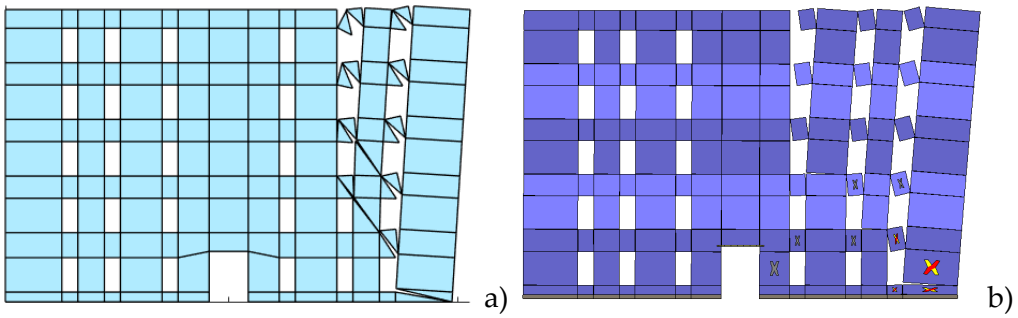

a) b)

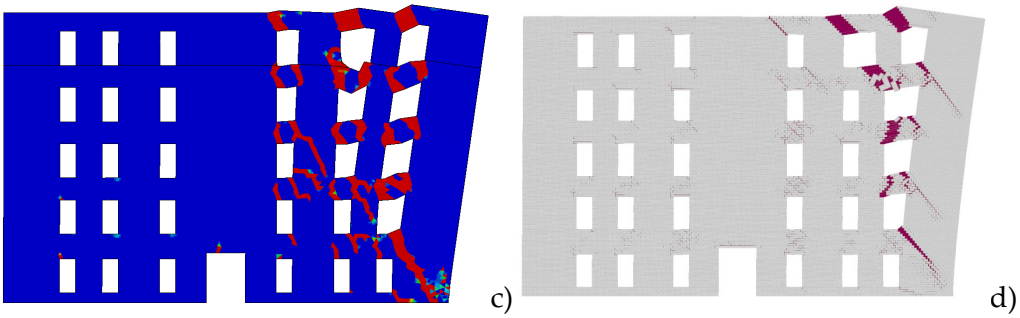


Figure 15 Collapse mechanisms of Configuration1

Figure 14 shows capacity curves that are signed by negligible softening effect. This is coherent with the collapse mode dominated by the rocking of peripheral walls. As the curves show, immediately after the peak value a short softening, due to the failures that involves the spandrel panels from top to bottom, is notices. At each failure, the capacity curve decreases. When all the spandrel panels, which are aligned along the same vertical, fail the right side of the wall collapses by rocking. This failure mode does not provide a significant softening, in absence of large displacement analyses, and the displacements increase almost under the same horizontal force. All the considered numerical strategies consistently describe the failure mechanism.

This kind of behaviour can occur for URM structure for which the connection of the slabs and their constraint effect can be considered insignificant.

### 5.2 Configuration2 - URM with elastic floor beams

A step forward in terms of more realistic configuration is represented by Configuration2 that introduces floor beams at each level except at the top edge of the wall. In this case, the beams are modelled as elastic elements.

In the limit analysis model, the concrete floor beams have been modelled as 1D rigid-plastic elements. In this model, the ultimate tensile strength is calibrated on the yielding value of all the reinforcement bars. The beam elements are perfectly connected to the masonry panels since no masonry-concrete interfaces have been modelled. Due to the fact that the adaptive NURBS-based limit analysis procedure was originally developed for unreinforced masonry structures only the reinforcement concrete elements can be currently taken into account in a simplified manner.

The DMEM approach simulates the interaction by means of discrete nonlinear interfaces between the plane macro-element and the beam element, as better specified in references [15].

In case of the homogeneous isotropic plastic-damaging 3D continuum model a conforming mesh is adopted, so that the 4-node tetrahedral elements related to masonry are fully connected with the ones related to concrete floor beam. In other words, a unique continuum is used and the mechanical properties are differentiated between masonry and concrete floor beam.

Lastly, the more sophisticated micromodelling approach uses 4-noded plane stress elements and forced based 1D fibre elements, for the concrete and the steel reinforcement bars, respectively. Concrete material is modelled with the damage model shown in section 3.3 and the properties of Table 2, steel reinforcement bars are modelled with Menegotto-Pinto's model [39] and the properties shown in Table 3

As Figure 16 reports, all the models reach similar base shear values (1841 kN, 1934 kN, and 1906 kN respectively). Consequently, the introduction of these beams, in this particular case, significantly changes the failure mechanism, compared to Configuration1, and the wall withstands globally to horizontal forces although the damage distribution is mainly located at the masonry piers of the ground elevation and at the spandrels at the upper floors, as can be observed by the collapse mechanisms reported in Figure 17. In this case, the floor beams guarantee the connection of all piers at the same level and increase the capacity of the spandrels. However, the concentration of damage at the first floor leads to a softening behaviour in terms of global ductility that is characterised by a softening branch in all the investigations. The result of the limit analysis shows a lower resistance compared to the outcomes of the pushover analyses.

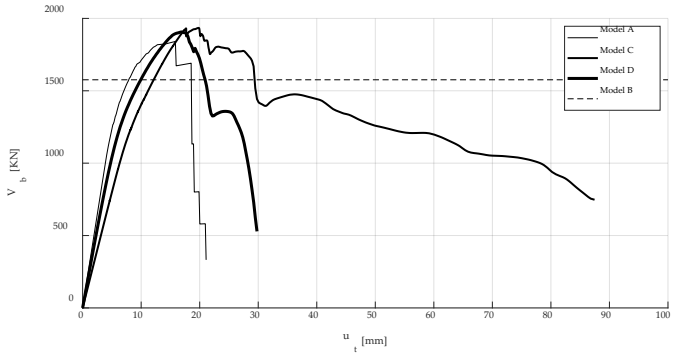


Figure 16 Comparison of the capacity curves obtained with three adopted software for Configuration2

As Figure 16 denotes, the major differences regard the softening branches. This aspect is crucial in case of seismic assessment and may affect the judgment on the seismic vulnerability of structures. Such results need additional investigation on the role of mechanical parameters that affect post peak behaviour.

The observation of the collapse mechanisms highlights shear failures at the piers of the ground floor and minor failures at the spandrels at the superior levels. All the models confirm the same collapse scenario.

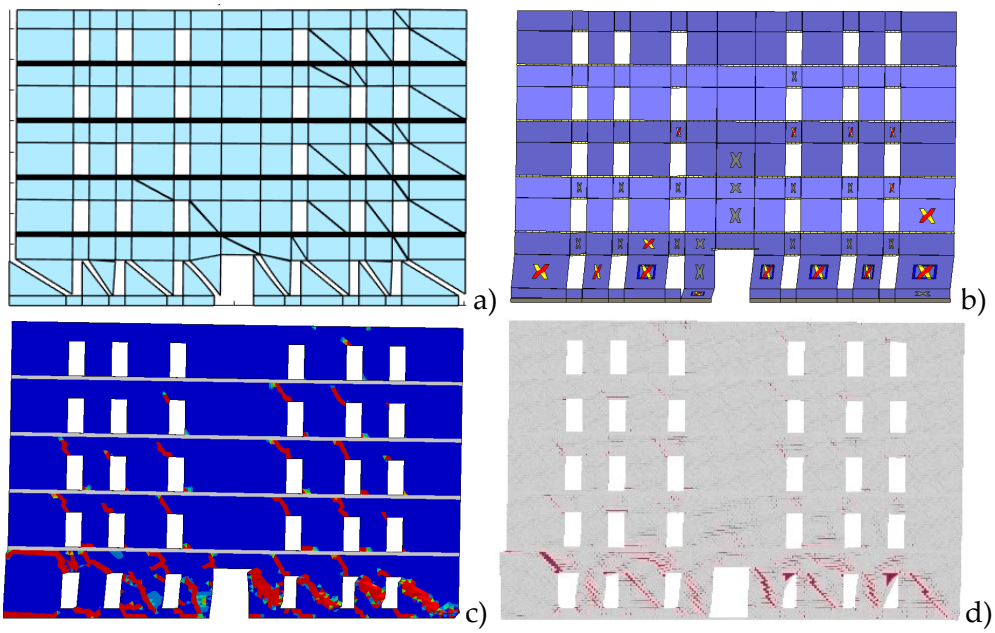


Figure 17 Collapse mechanisms of Configuration2

### 5.3 Configutation3 – URM with inelastic reinforced concrete floor beams and elastic lintel beams

The last comparison considers the inelasticity on the floor beams, Configuration3. The results are summarised in Figure 18 in terms of capacity curves. Globally similar peak values are reached by the models (1760 kN, 1576 kN, and 1586 kN). It is worth noting that the Configuration3 has not been modelled by the homogeneous isotropic plastic-damaging 3D continuum model. In contrast to the previous case (Configuration2) the nonlinear behaviour of the RC beam reduces the peak force and affects the collapse mechanism. As Figure 19 shows, the concrete floor beams are subjected to concentrated damage close to the lower corners of the openings at the lower levels leading, in some cases, to the shear failure of spandrel panels, as highlighted in Figure 19. As can be observed by Figure 19.a, the simplified strategy adopted for modelling the floor beams, previously described, does not predict their failure leading to a different collapse mechanism compared to those predicted by the other numerical simulations. Due to the absence of the floor beam at the top of the wall, failure of spandrels at the end level is also present. By comparing Figure 16 with Figure 18, it appears that the assumption of elastic behaviour for floor beams lead, on one hand, to an overestimation of the peak-values and, on the other hand, to a reduction of ductility.

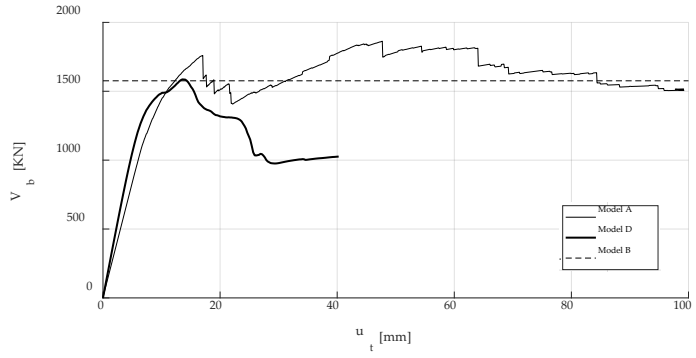


Figure 18 Comparison of the capacity curves obtained with two adopted software for Configuration3

Model A in Figure 18 exhibits a more ductile behaviour with respect to the detailed model, model D. As matter of fact, after the first peak value, the curve decreases due to the progressive failures of spandrel panels. At about 2.2 cm, several spandrel panels have reached their ultimate strength capacity. After this point, due to the fact that some spandrel panels at the upper floors can still resist to force increments, the rocking behaviour of peripheral pears introduce a hardening effect that characterizes the post-peak branch of the capacity curve.

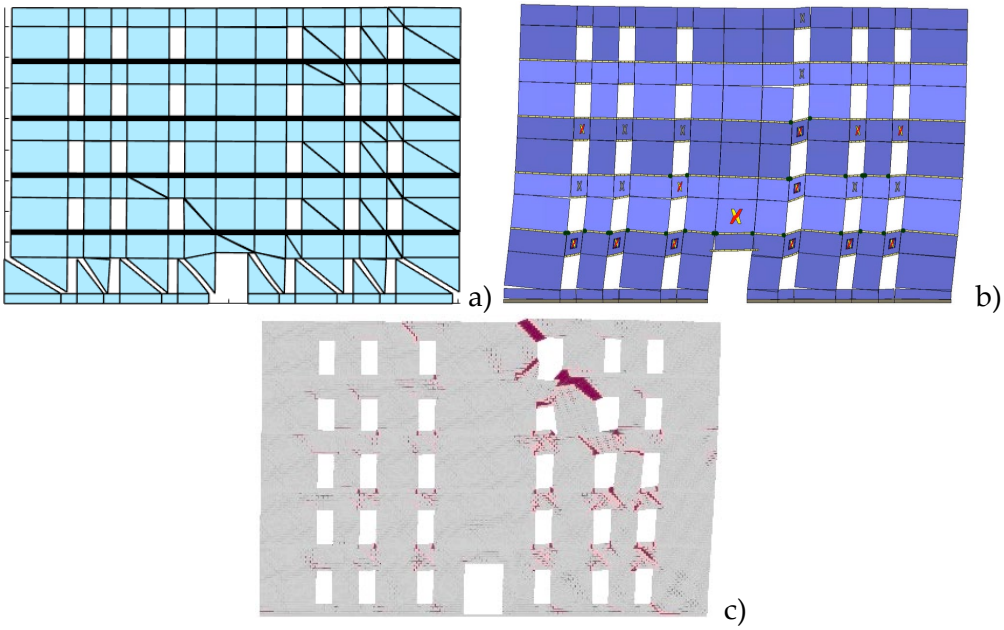


Figure 19 Collapse mechanisms of Configuration3

The results underline that accurate modelling approaches, that engages nonlinearities in all the structural elements, allow to better describe the collapse mechanism. As the failures at the last floor show, the presence of lintel beams only is not enough to avoid local failures. Detailed modelling strategies allows to accurately describe the failure mechanism, even though also less accurate models at the macro-scale, like model A, provide an satisfactory representation of the collapse mechanism.

The use of nonlinear concrete beams avoids the overestimation of peak forces and erroneous collapse behaviours. By comparing Figure 17 to Figure 19, can be observed that different collapse mechanisms affect the two cases. If the concrete model does not account for inelasticity an overstrength response of the spandrels can occur, this can alter the global behaviour leading to a localization of the damage at the ground level, Figure 17, as a consequence the complex nonlinear interaction between the spandrels and the floor beam is a key part of reliable modelling strategies for URM buildings.

Figure 20 compare the bending moments on the beam elements of Configuration2 (a) and Configuration3 (b) with reference to model A. In the picture, the red rectangles focus the attention on one of the panels denoted by different behaviour in the two cases. Due to the interaction between beams and masonry, nonlinear concrete

material model defines different forces distribution in the wall. When nonlinearity arises in beam elements the bending moments are equilibrated by the shear mechanics in the spandrel panels but they fail due to the shear force increments. As consequence, the entire multi-storey wall is involved in the collapse mechanism and the bending moments increase at the upper level (Figure 20.b). It is worth noting that all these aspects are influenced by the geometric and mechanical properties of concrete and masonry elements. Although an extensive parametric analysis was not performed aiming to achieve more general considerations, the result confirms that a reliable interaction between masonry walls and beam elements has to be guaranteed and nonlinear material model has to be always involved.

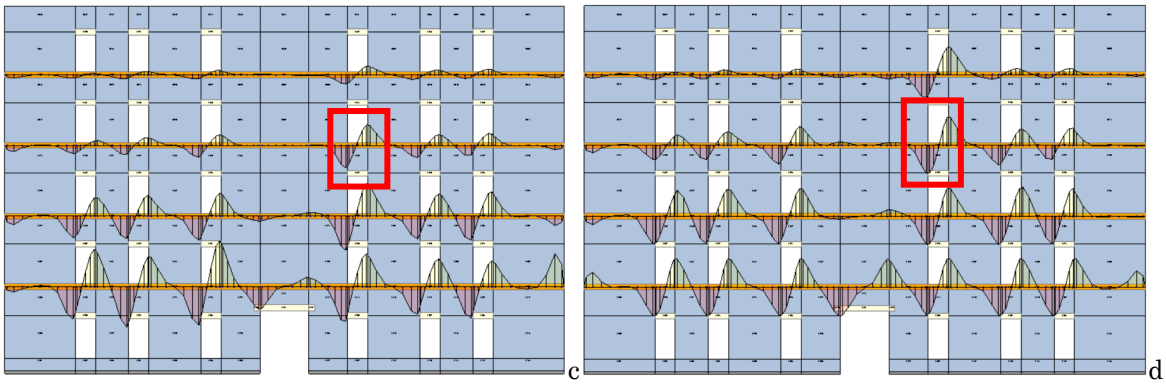


Figure 20 Bending moments in a) linear and b) nonlinear concrete floor beam at displacement of 1.83 cm of the control point (peak point of Configuration2)

## 6. Summary and Conclusions

Multi-storey masonry buildings represent a great percentage of the building stock in several countries. In this paper, the nonlinear behaviour of three configurations of a multi-storey wall has been investigated by means of mass proportional pushover analyses with different computational models, nonlinear limit analysis [9], planar discrete macroelements DME [3], continuum nonlinear FEM [10] and high fidelity nonlinear FEM micro-modelling [11] methods. The three benchmarks consider separately the contributes of concrete beams and the constitutive models (linear or nonlinear) in case of pushover analyses. In detail, Configuration1 does not consider floor beams; Configuration2 considers elastic floor beams at each level except to the roof level; Configuration3 considers nonlinear concrete floor beams and elastic lintel beams. The results of the analyses relative to the three different structural layouts have been discussed.

By considering the three configurations, the paper evaluates how the collapse mechanisms and, consequently, all the parameters that define a capacity curve (tangent stiffness, peak-force, softening branch, ultimate displacement) are influenced by the floor beams that affect the spandrel failure modes as well as the global mechanism. Though the influence of the stiffness ratio between concrete beams and masonry walls has not be investigated in this research, the paper arises the warning messages that the assumption of linear floor beams leads to the hazardous overestimation of the peak force values and unrealistic failure mechanisms. It is worth noting that in limit analysis theory materials are assumed rigid-perfectly plastic and, consequently, the effect of the elastic behaviour of single structural elements cannot be taken into account in any manner. Despite the simplicity and the limited computational burden needed to perform the analyses, important information in the pre-peak phase is lost, with consequent possible local and global discrepancies on the results when compared with those provided by more sophisticated approaches (see for instance collapse mechanisms depicted in Figure 19). The results relative to Configuration 2 and 3 confirm that a reliable interaction between masonry walls and beam elements has to be guaranteed to obtain a reliable collapse scenario.

The results of this paper have to be carefully considered if a reliable seismic assessment has to be performed on masonry multi-storey buildings.

## ACKNOWLEDGEMENTS

The study presented in the paper was developed within the research activities carried out in the frame of the 2014-2018 ReLUIS Project (Topic: Masonry Structures; Coord. Proff. Sergio Lagomarsino, Guido

Magenes, Claudio Modena, Francesca da Porto) and of the 2019-2021 ReLUIS Project - WP10 "Code contributions relating to existing masonry structures" (Coord. Guido Magenes). The projects are funded by the Italian Department of Civil Protection.

Moreover, the Authors acknowledge the whole group of research teams (RT) that participated to this research activity: UniGE RT (University of Genova; Coord. Prof. Serena Cattari; Participants: Stefania Degli Abbati, Daria Ottonelli); UniPV RT (University of Pavia: Coord. Guido Magenes, Participants: Carlo Manzini, Paolo Morandi); UniCH RT (University of Chieti-Pescara; Coord. Prof. Guido Camata, Participants: Corrado Marano); UniCT RT (University of Catania–Coord. Prof. Ivo Caliò; Participants: Francesco Canizzaro, Giuseppe Occhipinti, Bartolomeo Pantò); UniNA RT (University Federico II of Naples– Coord. Prof. Bruno Calderoni; Participants: Emilia Angela Cordasco); UniBO RT (University of Bologna- Coord. Prof. Stefano de Miranda – Participants: Giovanni Castellazzi, Antonio Maria D'Altri); POLIMI RT (Polytechnic of Milan- Coord. Prof. Gabriele Milani); IUAV RT (University of Venice - Coord. Prof. Anna Saetta; Participants: Luisa Berto, Diego Alejandro Talledo).

## REFERENCES

[1] S. Cattari, B. Calderoni, I. Caliò, G. Camata, S. de Miranda, G. Magenes, G. Milani and A. Saetta, "Nonlinear modelling of the seismic response of masonry structures: critical aspects in engineering practice," *Submitted to Bulletin of Earthquake Engineering, SI on "URM nonlinear modelling-Benchmark project"*, 2021a.

[2] D. Liberatore, Ed., Progetto Catania: indagine sulla risposta sismica di due edifici in muratura,, Roma: CNR-Gruppo Nazionale per la Difesa dai Terremoti, 2000, p. 275 .

[3] I. Caliò, M. Marletta and B. Pantò, "A simplified model for the evaluation of the seismic behaviour of masonry buildings," in *Proceedings of the 10th International Conference on Civil, Structural and Environmental Engineering Computing, Civil-Comp 2005*, 2005.

[4] S. Saloustros, L. Pelà and M. Cervera, "An Enhanced Finite Element Macro-model for the Realistic Simulation of Localized Cracks in Masonry Structures: A Large-Scale Application," *International Journal of Architectural Heritage,* 12 2017.

[5] D. Addessi, D. Liberatore and R. Masiani, "Force-Based Beam Finite Element (FE) for the Pushover Analysis of Masonry Buildings," *International Journal of Architectural Heritage,* vol. 9, no. 3, pp. 231-243, 4 2015.

[6] G. Milani, P. B. Lourenço and A. Tralli, "Homogenised limit analysis of masonry walls, Part II: Structural examples," *Computers & Structures,* vol. 84, no. 3, pp. 181-195, 2006.

[7] S. Cattari, G. Magenes, E. Spacone, I. Caliò, B. Calderoni, S. de Miranda, A. Saetta, G. Milani, S. Degli Abbati, D. Ottonelli, C. Manzini, P. Morandi, B. Pantò, F. Canizzaro, G. Occhipinti, A. Cordasco, G. Castellazzi, A. D'Altri, L. Berto, A. Doria and D. Talledo, "Progetto DPC-ReLUIS 2019-2021 – Uso dei software di calcolo nella verifica sismica degli edifici in muratura v1.0," 2020.

[8] S. Cattari and G. Magenes, "Benchmarking the software packages to model and assess the seismic response of unreinforced masonry existing buildings through nonlinear analyses," *submitted to the SI on URM nonlinear modelling - Benchmark project on Bulletin of Earthquake Engineering,* 2021.

[9] A. Chiozzi, G. Milani and A. Tralli, "A Genetic Algorithm NURBS-based new approach for fast kinematic limit analysis of masonry vaults,," *Computers and Structures,* vol. 182, p. 187–204, 2017.

[10] J. Lee and G. L. Fenves, "Plastic-Damage Model for Cyclic Loading of Concrete Structures," *Journal of Engineering Mechanics,* vol. 124, no. 8, p. 892–900, 1998.

[11] M. Petracca, *"Computational Multiscale Analysis of Masonry Structures",* Chieti, Italy: Ph.D. Thesis, Università degli Studi G. d'Annunzio di Chieti-Pescara,.

[12] G. Castellazzi, B. Pantò, G. Occhipinti, D. Talledo, L. Berto and G. Camata, "A comparative study on a complex URM building: part II—issues on modelling and seismic analysis part II—issues on modelling and seismic analysis," *Bulletin of Earthquake Engineering S.I.: URM NONLINEAR MODELLING - BENCHMARK PROJECT,* 2021.

[13] F. Cannizzaro, G. Castellazzi, N. Grillanda, B. Pantò and M. Petracca, "Modelling the seismic response of a 2-storey URM benchmark case study: Comparison among different modelling strategies using two- and three-dimensional elements," *submitted to Bulletin of Earthquake Engineering S.I.: URM NONLINEAR MODELLING - BENCHMARK PROJECT, 2021,* 2021.

[14] NTC18, "NTC Normativa tecnica per le costruzionii - DM 14 Gennaio 2018," MINISTERO DELLE INFRASTRUTTURE E DEI TRASPORTI, 2018.

[15] I. Caliò and B. Pantò , "A macro-element modelling approach of Infilled Frame Structures," *Computers and Structures,* vol. 143, pp. 91-107, 2014.

[16] C. Chácara, F. Cannizzaro, B. Pantò, I. Caliò and P. Lourenço, "Assessment of the dynamic response of unreinforced masonry structures using a macro-element modeling approach," *Earthquake Engineering & Structural Dynamics,* vol. 47, no. 12, pp. 2426-2446, 2018.

[17] S. Caddemi, I. Caliò, F. Cannizzaro and B. Pantò, "A new computational strategy for the seismic assessment of infilled frame structures," in *Civil-Comp Proceedings*, 2013.

[18] B. Pantò, I. Caliò e P. Lourenco, «A 3D discrete macro-element for modelling the out-of-plane behaviour of infilled frame structures,» *Engineering Structures,* vol. 175, pp. 371-385, 23 8 2018.

[19] R. Haupt and S. Haupt, Practical Genetic Algorithms, New York: John Wiley & Sons, 1998.

[20] N. Grillanda, A. Chiozzi, G. Milani and A. Tralli, "Collapse behavior of masonry domes under seismic loads: an adaptive NURBS kinematic limit analysis approach," *Engineering Structures,* vol. 200, 2019.

[21] N. Grillanda, M. Valente and G. Milani, "ANUB-Aggregates: a fully automatic NURBS-based software for advanced local failure analyses of historical masonry aggregates," *Bulletin of Earthquake Engineering,* vol. 18, p. 3935–3961, 2020.

[22] S. Tiberti, N. Grillanda, G. Milani and V. Mallardo, "A Genetic Algorithm adaptive homogeneous approach for evaluating settlement-induced cracks in masonry walls," *Engineering Structures,* vol. 221, 2020.

[23] A. Mirmiran and M. Shahawy, "Dilation characteristics of confined concrete," *Mechanics of Cohesive-frictional Materials,* vol. 2, no. 3, p. 237–249, 1997.

[24] G. Milani, M. Valente and C. Alessandri, "The Narthex of the Church of the Nativity in Bethlehem: A Non-Linear Finite Element Approach to Predict the Structural Damage," *Computers & Structures,* vol. 207, pp. 3-18, 2018.

[25] A. M. D'Altri, F. Messali, J. Rots, G. Castellazzi and S. de Miranda, "A damaging block-based model for the analysis of the cyclic behaviour of full-scale masonry structures," *Engineering Fracture Mechanics,* vol. 209, pp. 423-448, 2019.

[26] J. Lubliner, J. Oliver, S. Oller and E. Oñate, "A Plastic-Damage Model for Concrete," *International Journal of Solids and Structures,* vol. 25, no. 3, p. 299–326, 1989.

[27] G. Fortunato, M. Funari and P. Lonetti, "'Survey and seismic vulnerability assessment of the Baptistery of San Giovanni in Tumba (Italy),," *Journal of Cultural Heritage,* vol. 26, pp. 64-78., 2017.

[28] A. M. D'Altri and S. de Miranda, " Environmentally-induced loss of performance in FRP strengthening systems bonded to full-scale masonry structures.," *Construction and Building Materials,* vol. 249, 2020.

[29] L. Berto, A. Saetta, R. Scotta and R. Vitaliani, "An orthotropic damage model for masonry structures.," *International Journal for Numerical Methods in Engineering,*, vol. 55, no. 2, pp. 127-157, 2002.

[30] L. Pelà, M. Cervera and P. Roca, "An orthotropic damage model for the analysis of masonry structures.," *Construction and Building Materials* , vol. 41, pp. 957-967, 2013.

[31] A. D'Altri, F. Cannizzaro, M. Petracca and D. Talledo, "Nonlinear modelling of the seismic response of masonry structures: Calibration strategies," *Bulletin of Earthquake Engineering in SI "URM nonlinear modelling-Benchmark project",* 2021.

[32] M. Cervera, J. Oliver and R. Faria, "Seismic evaluation of concrete dams via continuum damage model," *Earthquake engineering & structural dynamics,*, vol. 24, no. 9, pp. 1225-1245, 1995.

[33] R. Faria, J. Oliver and M. Cervera, "A strain-based plastic viscous-damage model for massive concrete structures," *International Journal of Solids and Structures,* vol. 35, no. 14, pp. 1533-1558, 1998.

[34] J. Wu, J. Li and R. Faria, "An energy release rate-based plastic-damage model for concrete," *International Journal of Solids and Structures,* vol. 43, no. 3, pp. 583-612, 2006.

[35] M. Petracca, L. Pelà, R. Rossi, S. Zaghi, G. Camata and E. Spacone, "Micro-scale continuous and discrete numerical models for nonlinear analysis of masonry shear walls," *Construction and Building Materials,* vol. 149, p. 296–314, 2017.

[36] M. Petracca, L. Pelà, R. Rossi, S. Oller, G. Camata and E. Spacone, "Multiscale computational first order homogenization of thick shells for the analysis of out-of-plane loaded masonry walls," *Computer Methods in Applied Mechanics and Engineering,* vol. 315, pp. 273-301, 2017.

[37] M. Petracca, L. Pelà, R. Rossi, S. Oller, G. Camata and E. Spacone, "Regularization of first order computational homogenization for multiscale analysis of masonry structures," *Computational mechanics,* vol. 57, no. 2, pp. 257-276, 2016.

[38] J. Lubliner, J. Oliver, S. Oller and E. Onate, "A plastic-damage model for concrete," *Int. J. Solids Struct,* vol. 25, no. 3, pp. 299-326, 1989.

[39] M. Menegotto e P. Pinto, «Method of analysis of cyclically loaded RC plane frames including changes in geometry and non-elastic behavior of elements under normal force and bending.,» *Preliminary Report IABSE,* vol. 13, 1973.

581

582